Isolation and Structural Characterization of Monomeric and Trimeric Photosystem I Complexes (P700·FA/FB and P700·Fx) from the Cyanobacterium Synechocystis PCC 6803

Kruip, Jochen; Boekema, Egbert J.; Bald, Dirk; Boonstra, Arjen F.; Rögner, Matthias

Published in:
Default journal

Publication date:
1993

THE JOURNAL OF BIOLOGICAL CHEMISTRY
Vol. 268, No. 31, Issue of November 5, pp. 23353–23360, 1993
Printed in U.S.A.

Isolation and Structural Characterization of Monomeric and Trimeric Photosystem I Complexes (P700·F_A/F_B and P700·F_X) from the Cyanobacterium *Synechocystis* PCC 6803*

(Received for publication, July 7, 1993)

Jochen Kruip‡, Egbert J. Boekema§, Dirk Bald‡, Arjen F. Boonstra§, and Matthias Rögner‡¶

From the ‡Institute of Botany, University of Münster, Schlossgarten 3, D-48149 Münster, Germany and the §BIOSON Research Institute, Biophysical Chemistry, University of Groningen, Nijenborgh 4, 9747 AG Groningen, The Netherlands

An isolation procedure was developed for the cyanobacterium *Synechocystis* 6803 (and 6714) which yields both monomeric and trimeric photosystem I complexes (P700·F_A/F_B complexes) depleted of the stroma-exposed subunits PsaC, -D, and -E (P700·F_X complexes). Analysis by high resolution gel electrophoresis in combination with immunoblotting and N-terminal sequencing reveals the selective and quantitative removal of PsaC, -D, and -E from the P700·F_A/F_B complex, containing PsaA, -B, -C, -D, -E, -F, -K, -L and at least two subunits ≤4 kDa. Monomeric and trimeric P700·F_X complexes show an identical subunit composition and an identical charge recombination half-time of 750 ± 250 μs as determined by flash-induced absorption change measurements, reflecting the quantitative loss of iron-sulfur clusters F_A/F_B and the presence of cluster F_X. The existence of a stable trimeric P700·F_X complex enables a detailed structural analysis by electron microscopy with high resolution. Comparison of averaged top and side view projections of P700·F_X and P700·F_A/F_B complexes show that the height of the complex is reduced by about 2.5–3.3 nm upon removal of the three stroma-exposed subunits and indicate the position of these three subunits on the PS I surface. While the outer contours of the stroma exposed mass of PS I agree very well with the three-dimensional crystal analysis recently published for trimeric PS I of *Synechococcus elongatus* (Krauss, N., Hinrichs, W., Witt, I., Fromme, P., Pritzkow, W., Dauter, Z., Betzel, C., Wilson, K. S., Witt, H. T., and Saenger, W. (1993) *Nature* 361, 326–330), only the structural analysis presented here is able to assign the stroma-exposed mass exclusively to the subunits PsaC, -D, and -E and to exclude a contribution of other subunits.

Photosystem I (PS I)[1] is one of the two pigment-protein complexes of oxygenic photosynthesis in green plants, algae, and cyanobacteria. PS I catalyzes the light-dependent transfer of electrons from reduced plastocyanin or cytochrome c_{553} to soluble ferredoxin (see Refs. 1–4, for reviews). In cyanobacteria the native PS I complex has been shown to consist of 12 different subunits which have been named PsaA through PsaN, with PsaG and PsaH missing as they can be found only in higher plants (4, 34). The extrinsic subunits PsaC, -D, and -E are localized at the stromal side and PsaF at the lumenal side of the thylakoid membrane, whereas all other subunits seem to be intrinsic membrane proteins. The PsaA/PsaB heterodimer harbors the primary electron donor P700 (a chlorophyll dimer) and the electron acceptors A_0 (a monomeric chlorophyll), A_1 (a phylloquinone), and F_X (a [4Fe4S] iron-sulfur cluster); therefore, the heterodimer is both the site of charge separation and of subsequent charge stabilization (2). Also it binds most of the antennae chlorophyll molecules. PsaC contains the two iron-sulfur clusters F_A and F_B which serve as electron acceptors (2). PsaD and PsaF have been shown to be candidates for ferredoxin docking (5, 6) and plastocyanin (or cytochrome c_{553}) docking (7, 8), respectively. The function of the other subunits remain unknown at the moment.

Golbeck *et al.* (9) reported a preparation of PS I (termed PS I core protein or P700-F_X, respectively) from the mesophilic cyanobacterium *Synechococcus* PCC 6301, which has lost PsaC, -D, and -E upon treatment with chaotropes. Concomitant with the loss of these subunits was the loss of the iron-sulfur clusters F_A and F_B as demonstrated by EPR spectroscopy (10). The ability to reconstitute the P700·F_X complex with purified PsaC, -D, and -E has enabled the functional study of these subunits by site-directed mutagenesis (11, 12). However, up to now no structural studies have been performed with this P700·F_X complex. It is unknown whether this preparation is homogeneous or whether oligomeric P700·F_X complexes can exist, and if so, whether they differ in function from the monomeric P700·F_X complex.

From cyanobacteria, PS I has been isolated both as a monomeric and as a trimeric complex (13, 30); however, up to now it is unknown, which form exists *in vivo* (19, 28). Purified monomeric and trimeric P700·F_A/F_B complexes of cyanobacteria have been studied by electron microscopy both as individual complexes (15, 17, 30) and as two-dimensional crystals (18, 19). From tilt series of two-dimensional P700·F_A/F_B crystals of *Synechococcus* sp. a low resolution three-

* This work was supported by the Netherlands Foundation for Chemical Research (SON) with financial aid from the Netherlands Organization for Scientific Research (NWO), by the Deutsche Forschungsgemeinschaft (Ro 858/2-1), and by a grant from the North-rhine-Westfalian Ministry of Science and Research (Bennigsen-Foerder prize, awarded to M. R.). The costs of publication of this article were defrayed in part by the payment of page charges. This article must therefore be hereby marked "*advertisement*" in accordance with 18 U.S.C. Section 1734 solely to indicate this fact.

¶ To whom correspondence should be addressed: Institute of Botany, University of Münster, Schlossgarten 3, D-48149 Münster, Germany. Tel.: 0049-251-833803; Fax: 0049-251-833823; E-mail: ROGNER@DMSWWU1A. (Bitnet).

[1] The abbreviations used are: PS, photosystem; CAPS, (3-[cyclohexylamino]-1-propane sulfonic acid; HPLC, high performance liquid chromatography; MSA, multivariate statistical analysis; P700, primary electron donor of PS I; Pcc, Pasteur culture collection; Psa, photosystem I protein (PS I nomenclature); P700·F_X, PS I complex without PsaC, -D, and -E (electron transfer up to F_X); P700·F_A/F_B, native PS I complex (electron transport up to F_A/F_B); PAGE, polyacrylamide gel electrophoresis.

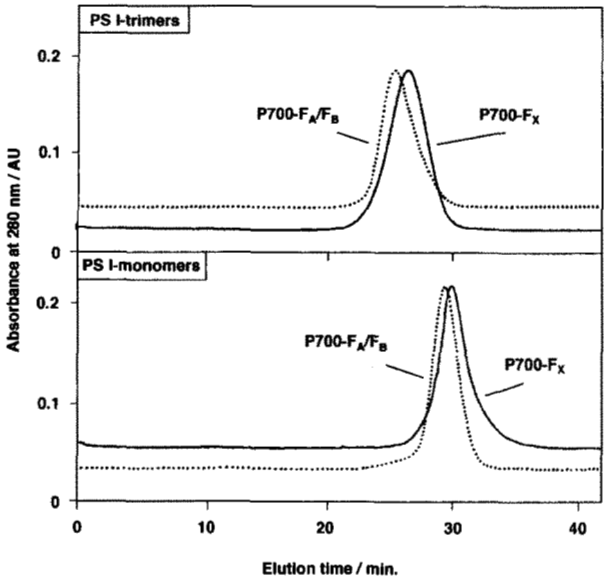

FIG. 1. **Elution profile of purified PS I complexes from an HPLC gel filtration column (Superose 6).** Monomeric and trimeric P700·F_X complexes (*full line*) had been pre-purified, after urea treatment, on the same column; chromatograms of the corresponding monomeric and trimeric P700·F_A/F_B complexes (*dashed line*) are shown for comparison. The flow rate was 0.5 ml/min and absorbance was recorded at 280 nm.

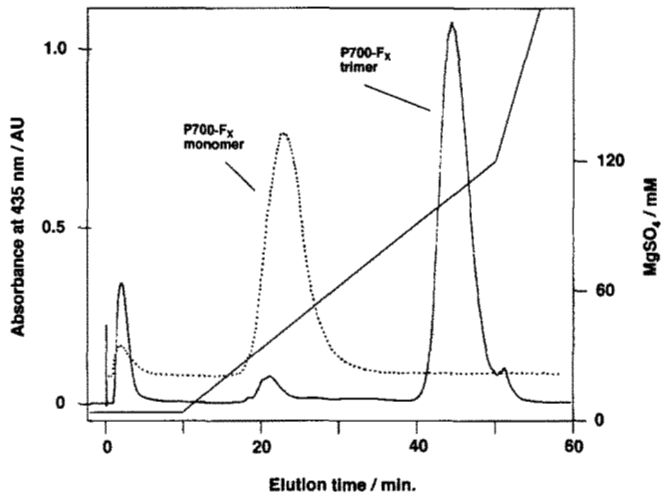

FIG. 2. **Purification of P700·F_X complexes on an anion-exchange column (Mono Q HR 5/5).** The elution profile shows monomeric (*dashed line*) and trimeric (*full line*) P700·F_X complexes, obtained after urea treatment (see "Materials and Methods"), on a linear $MgSO_4$ gradient. The flow rate was 0.5 ml/min and absorbance was recorded at 280 nm.

dimensional model was reconstructed (18). Even more information has recently been gained from three-dimensional crystals of trimeric P700·F_A/F_B from *Synechococcus* sp. with 6-Å resolution by x-ray structure analysis (33, 35). The outer contours of the complex, the position of the three iron-sulfur centers, most of the α-helices, many pigments and, presumably, the special pair could be determined.

Starting from a preparation of pure and homogeneous monomeric and trimeric P700·F_A/F_B complexes (36), we describe here a modified procedure for the generation of highly purified and homogeneous monomeric and trimeric P700·F_X complexes of *Synechocystis* 6803. Functional and structural homogeneity of these PS I complexes is shown by a detailed analysis of the subunit composition, by HPLC gel filtration and kinetics of charge recombination. Electron microscopy in combination with image analysis reveals characteristic differences between top and side views of trimeric P700·F_A/F_B and P700·F_X complexes and indicates the localization of the three stromal subunits PsaC, -D, and -E on the surface of PS I. This structural analysis also shows for the first time that only these subunits protrude from the membrane at the stroma side and that this protrusion disappears completely with the selective and quantitative removal of the subunits presented in this paper.

MATERIALS AND METHODS

Isolation of the P700·F_A/F_B Complex—Growth conditions of *Synechocystis* PCC 6803 (glucose-tolerant and phycocyanin-deficient strain) and isolation of the thylakoid membranes were described earlier (13). Extraction of membrane proteins and subsequent sucrose density gradient centrifugation yielded two green bands from which further purification of monomeric and trimeric PS I complexes was done by HPLC techniques as described in Refs. 13 and 14. For HPLC, a Waters system (2 pumps, model 510, controller, model 680, and a Rheodyne injector, model 7161) in combination with a dual wavelength absorbance detector (Visi Duo; Latek Co., Germany) was used. The HPLC columns were kept at a constant temperature of 10 °C in an oven compartment (Beckman Co.). Similar to Ref. 13, an anion exchange chromatography step (HiLoad Q-Sepharose HP 16–10; Pharmacia, Sweden) was used followed, after buffer exchange, by a hydroxyapatite chromatography step (Superformance hydroxyapatite 50–10; Merck, Germany).

Isolation of the P700·F_X Complexes—Purified P700·F_A/F_B complexes (200 μg of chlorophyll/ml) were incubated for 35 min in 6.8 M urea (20 mM CAPS, pH 10) similar to Ref. 9. Excess urea was quickly removed by a desalting column (EconoPac 10DG; Bio-Rad). Detached subunits and aggregated complexes were removed by either a gel-filtration column (Superose 6; Pharmacia, Sweden) or on an anion-exchange column (Mono Q HR 5/5; Pharmacia, Sweden).

Biochemical Standard Techniques—SDS-PAGE was done according to Schägger and von Jagow (21). UltroScan XL with GelScan software (Pharmacia, Sweden) was used for densitometric analysis of Coomassie-stained gels. For immunoblotting and N-terminal sequencing proteins were electroblotted (Fastblot; Biometra, Germany) onto a polyvinylidene difluoride membrane (Immobilon; Millipore) as in Ref. 22. Immunochemical detection using alkaline phosphatase conjugated to an anti-rabbit antibody was carried out as in Ref. 13. Antibodies against the PsaC, -D, and -E proteins were kindly provided by Dr. J. Golbeck (University of Nebraska, Lincoln), a PsaF antibody was a kind gift from Dr. R. Malkin (University of California, Berkeley). N-terminal sequencing was performed by Eurosequence, Groningen, on an Applied Biosystems 477A Protein Sequencer. Data base searching and sequence alignment was done with the HUSAR program package (DKFZ, Heidelberg, Germany).

Spectroscopic Methods—Absorbance spectra were recorded on a Hitachi U2000 spectrophotometer. Chlorophyll concentration was determined using an extinction coefficient of 74,000 M^{-1} cm^{-1} at 679 nm. Flash induced absorption changes were measured according to Ref. 23. Linear dichroism and 77K OD spectra were recorded as in Ref. 24.

Electron Microscopy and Image Analysis—Specimens for electron microscopy were prepared by the droplet technique using 1% uranyl acetate as a negative stain. Electron microscopy was performed with Philips EM 400 and Jeol JEM 1200 EX electron microscopes. From 13 micrographs of P700·F_A/F_B complexes digitized with a Kodak Eikonix Model 1412 CCD camera we selected 898 top view projections in a format of 72 × 72 pixels. From 14 digitized micrographs of P700·F_X complexes, 391 top view projections and 94 side view projections were selected in a format of 64 × 64 pixels. A scan step size of 23.8 μm, corresponding to a pixel size of 0.40 nm at the specimen level, was used for P700·F_A/F_B micrographs and of 25.5 μm (0.46 nm) for the P700·F_X micrographs. For comparison with the P700·F_A/F_B images, the P700·F_X images were enlarged after analysis with a factor 1.20 and set to the 72 × 72 format.

Image analysis was carried out on a Convex C220 computer using IMAGIC software. In the first step all selected top view images were band-pass filtered to remove the very high and suppress the very low frequency components. In the next step the images were aligned with

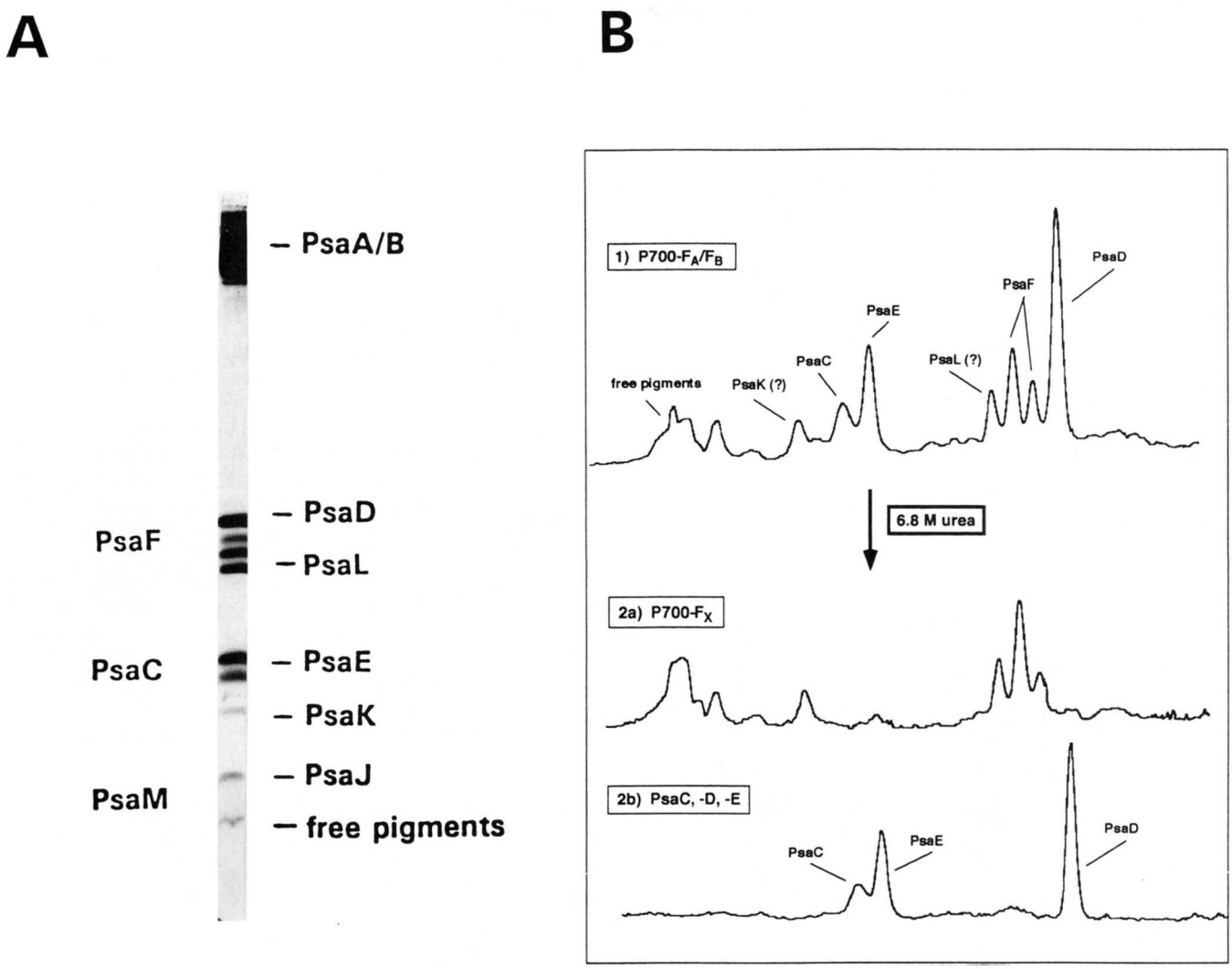

FIG. 3. *A*, SDS-PAGE of trimeric P700·F_A/F_B complex after purification according to Ref. 14. *B*, densitometric scans of gels after SDS-PAGE showing proteins below 20 kDa (PsaA/B heterodimer with an apparent molecular mass of 60–65 kDa has been omitted). The *upper lane* shows the band pattern of the trimeric P700·F_A/F_B complex, the *middle* one the purified trimeric P700·F_X complex, and the *lower* one the proteins lost due to the urea treatment.

correlation techniques, starting with one noisy single projection as a first reference. Intermediate references were constructed from the sums of the best aligned PS I complexes from previous alignments (16). Before the last alignment step, the prealigned projections were 3-fold symmetrized, and in the symmetrized form an additional rotational alignment was performed. In the last steps, the aligned 3-fold symmetrized PS I complexes were submitted to multivariate statistical analysis (MSA) and automatic classification. These steps were carried out essentially as described previously (15, 16). Finally the members of each class were summed. For comparison of final sums (of combined classes), the low frequency components of these images, earlier suppressed by band-pass filtering, were reset to their original value. For generating contour plots, the images were interpolated to a 512 × 512 pixel format.

Chemicals—Dodecyl-β-D-maltoside was purchased from Biomol (Germany), urea from U. S. Biochemical Corp. (Germany), CAPS, 2,6-dichlorophenolindophenol, methyl viologen, fast red and napthol AS-Bi phosphate from Sigma, and an anti-rabbit antibody from Bio-Rad. All other reagents were of analytical grade.

RESULTS

Isolation of the P700·F_X Complex—Starting from purified P700·F_A/F_B complexes, extremely pure and homogeneous monomeric and trimeric P700·F_X complexes could be prepared simply by incubating P700·F_A/F_B complexes in 6.8 M urea followed by an additional HPLC step. This shows that urea treatment does not destroy the trimeric form of the PS I complex.

For the final purification step we developed two different procedures: HPLC of the incubation mixture on a gel filtration column (Superose 6) yielded pure and homogeneous P700·F_X complexes as shown by rechromatography (Fig. 1). Due to the loss of PsaC, -D, and -E a clear shift in the apparent molecular mass of the P700·F_X complexes (Fig. 1, *full line*) relative to the P700·F_A/F_B complexes (*dashed line*) can be seen.

Alternatively we used an anion-exchange column (Mono Q) for the final purification. Fig. 2 shows the separation of monomeric and trimeric P700·F_X complexes by a linear gradient of $MgSO_4$. Due to the urea treatment, the trimeric P700·F_X complex contains some residual monomeric complexes (*full line*), while the monomeric one still contains some oligomeric material, possibly aggregates (*dashed line*). As these components are sufficiently well separated in the elution profile, with this method also pure and homogeneous P700·F_X complexes can be obtained. Moreover, scaling up of this step by a factor of 10 is possible by using a Q-Sepharose HiLoad column.

The same procedure for the preparation of monomeric and trimeric P700·F_X complexes was applied to the cyanobacterium *Synechocystis* PCC 6714 yielding identical results (data not shown). This shows the reproducibility and versatility of this method.

Subunit composition of P700·F_A/F_B and P700·F_X Complexes—The subunit composition of the different isolated PS I complexes was determined by PAGE, using high resolution gels in the molecular mass range below 20 kDa (Fig. 3*A*). The P700·F_A/F_B complexes contain PsaA, -B, -C, -D, -E, -F, -K, -L and possibly two or three smaller proteins (presumably PsaI/-J and -M), similar to Ref. 37. However, N-terminal sequences of the bands at 14.5 and 15.5 kDa are identical with the deduced protein sequence of PsaF from *Synechocystis* PCC 6803 (26), although both protein bands do not cross-react with an antibody against spinach PsaF (data not shown). N-terminal sequencing suggests that the protein at 13.6 kDa is PsaL showing highest homology (77%) to PsaL from barley (Table I). Also, in contrast to all other subunits the amount of this subunit seems to be reduced in the monomeric forms by about 50% (data not shown).

Densitometric scans (Fig. 3*B*) clearly show that urea treatment specifically and quantitatively removes PsaC, -D, and -E from monomeric and trimeric P700·F_A/F_B complexes.

Spectroscopic Characterization of the P700·F_X Complex—Flash-induced absorption change measurements show that loss of PsaC, -D, and -E leads to a decrease in charge recombination half-times from 25 ms, corresponding to the $P700^+(F_A/F_B)^-$ backreaction (10), to (750 ± 250) μs, consistent with the $P700^+F_X^-$ backreaction and the loss of Fe-S clusters F_A and F_B (10). Comparison of the amplitude of the absorbance change at different time resolution (up to ns range) indicate only a very small loss of Fe-S cluster F_X (utmost 10–15%), yielding a component with $t_{½}$ = 10–30 μs due to charge recombination between $P700^+$ and A_1^- (20). Remainders of a slow phase (10% with $t_{½}$ > 20 ms) most probably are due to electron transfer with oxygen as acceptor.[2]

Linear dichroism and 77 K OD spectra are essentially the same for both monomeric and trimeric P700·F_A/F_B complexes and the corresponding P700·F_X complexes (data not shown). In addition, the number of chlorophylls is identical in both PS I complexes: 90 ± 10 chlorophyll/P700.

Structural Analysis of the Trimeric P700·F_A/F_B Complex by Electron Micrography—Although electron micrographs of both monomeric and trimeric P700·F_A/F_B complexes and P700·F_X complexes were obtained, only trimeric PS I complexes are shown as they were more suitable for image analysis, due to their larger dimensions. Fig. 4*A* shows such an electron micrograph of trimeric P700·F_A/F_B complexes in top and side view position. The *inset* shows a selected part with stacked side views of double trimers. It is evident that the spacing within one double trimer (indicated by *2 white* or *black arrows*, respectively) is larger than the spacing between two double trimers.

From the electron micrographs, 898 top view projections

TABLE I

N-terminal sequence of PsaL from Synechocystis PCC 6803

The PsaL protein from *Synechocystis* has been compared with known sequences from other organisms. The dash indicates a gap introduced to optimize alignment. Vertical lines show identical amino acids, whereas colons indicate conservative amino acid replacements. References: Barley (25), *Anabaena* 29413 (26), *Synechococcus* 7002 (10), *S. elongatus* (27).

S. elongatus	MAE ELVKPYNGPD
	: ::| ||
Synechocystis **6803**	**AESN QVVQAYN**
	:: |||| |
Barley	KAVKSDKPTQ QVVQPINGDP
	: || || | ||
Anabaena 29413	/NLPSDPRNR EVVFPAGRDP
	::: :| ||
Synechococcus 7002	M DIIQHGG-DP

[2] J. Golbeck, personal communication.

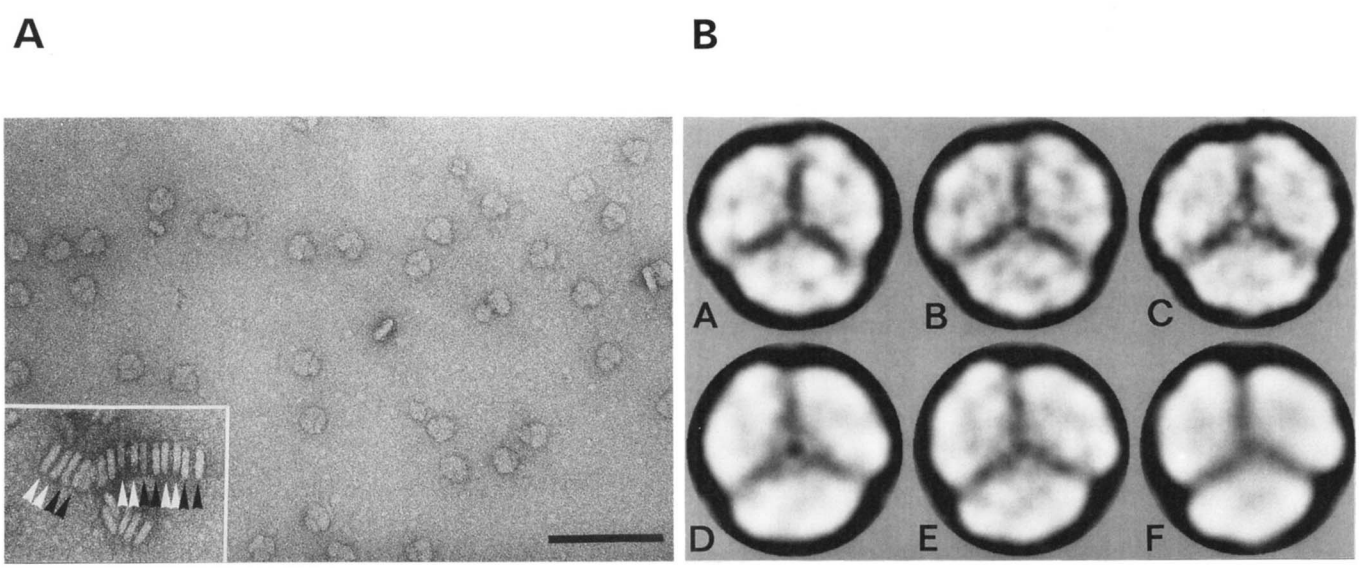

FIG. 4. **Electron microscopy and image analysis of the trimeric P700·F_A/F_B complex.** *A*, part of an electron micrograph showing P700·F_A/F_B complexes in top and side view position. The PS I complexes were negatively stained with a 1% solution of uranyl acetate. *Inset*, selected side views of trimeric P700·F_A/F_B complexes. Double trimers are indicated by a pair of *white* and *black arrows*, respectively. The *bar* represents 100 nm. *B*, image analysis of 898 top view projections of the P700·F_A/F_B complex. The final classification yields a decomposition into six classes with 137 (*A*), 139 (*B*), 87 (*C*), 123 (*D*), 91 (*E*), and 151 (*F*) members, respectively. Note: the images are shown with the imposed band-pass filter, which is necessary for the suppression of unwanted noise during analysis. The filter suppresses the central density of the trimer as well as the center of each monomer, but the features of fine details, such as the knobs in the center of the trimers, are enhanced.

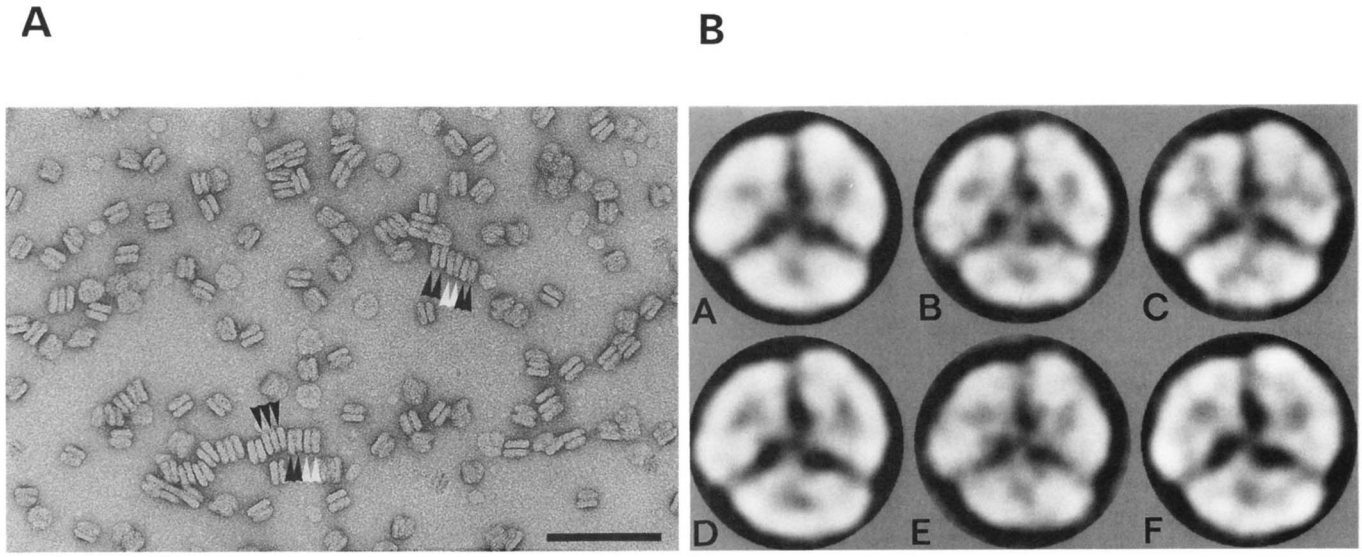

FIG. 5. **Electron microscopy and image analysis of the trimeric P700·F_X complex.** *A*, part of an electron micrograph showing P700·F_X complexes in top and side view positions. *Arrows* indicate side views of trimeric P700·F_X complexes. The *three black arrows* mark side views selected for image processing (see Fig. 7). The PS I complexes were negatively stained with a 1% solution of uranyl acetate. The *bar* represents 100 nm. *B*, image analysis of 391 top view projections of P700·F_X complexes. The final classification yields a decomposition into six classes with 46 (*A*), 56 (*B*), 48 (*C*), 38 (*D*), 36 (*E*), and 51 (*F*) members, respectively. Note: the images are shown with the imposed band-pass filter, as in Fig. 4*B*, and on the same scale.

were selected for computer processing. In the first cycle of alignment, MSA, and classification, most of the projections could already be separated into two distinct groups representing upside-up ("flip") and upside-down ("flop") attachment of the PS I complexes on the carbon support film. The best flip and flop class from the first classification were used as reference for the next alignment procedure. After three subsequent cycles of alignment, MSA, and classification steps, the data set could be fully separated into two groups of projections. In the last classification the data set was decomposed into six classes (Fig. 4*B*), each of them with a distinct handedness. Three classes represent projections of the flip type (Fig. 4*B*, *A-C*), the other three the flop type (Fig. 4*B*, *D-F*). All flip classes have three small knobs in the center of the trimer; as they show only minor differences they could be combined for the final sum of the flip class. When the best 50% of the PS I complexes of each class (*i.e.* those with the highest correlation coefficient) were summed, Fig. 6*A* resulted. In this image, too, three masses in the center of the trimer can be seen. In comparison to the flip classes, the flop classes are more heterogeneous; in the classes D and F of Fig. 4*B*, the fine structure is partly lost. Therefore in the final flop image only the best 65 members of class E of Fig. 4*B* were combined yielding Fig. 6*B*. In this case, the image of three masses in the center of the trimer is weak or missing.

Structural Analysis of the Trimeric P700·FX Complex by Electron Micrography—Fig. 5*A* shows an electron micrograph of trimeric P700·F_X complexes in top and side view position. It also shows side views arranged in stacks similar to the P700·F_A/F_B complex (Fig. 4*A*, *arrows*). However, in contrast to the P700·F_A/F_B complex the gaps between all trimers are roughly similar and distinctly smaller, which enables image processing.

Image processing of 391 top view projections was carried out in a similar way to the P700·F_A/F_B complex. After two cycles of alignment, MSA, and classification, the data set was also decomposed into six classes (Fig. 5*B*). In contrast to the P700·F_A/F_B complex, the P700·F_X complexes are almost all in the flip position as is evident from the three small knobs in the center of the trimer. Among the six classes no flop class can be found. A visual examination of all individual 3-fold averaged projections revealed only very few clear flop projections. Apparently their amount is too small to form a class of their own. As for the P700·F_A/F_B complex, some of the classes (such as *A* and *F* in Fig. 5*B*) showed no fine details. In classes B and E, the three small knobs in the center can be seen exactly at the same position as in the flip views of the P700·F_A/F_B complex (Fig. 4*B*, *A-C*). This is more evident in the final flip image (Fig. 6*C*) which was made of the best 47 projections of class B of Fig. 5*B*, the class with the best preserved fine structure. This final flip image of the P700·F_X complex shows oval stain pits in between of the monomers which are distinctly larger than the corresponding ones in the flip view of the averaged P700·F_A/F_B complex (Fig. 6*A*).

To visualize the difference between flip images of the P700·F_A/F_B complex and the P700·F_X complex (Fig. 6, *A* and *C*), the images were subtracted. The contour version of this difference image (with the strongest differences contoured by 4 levels) was then superimposed on the image of the P700·F_X complex (Fig. 6*D*). This figure shows relevant differences only in the center of the monomers and indicates the location of the three missing subunits in the center of the monomer slightly shifted to the center of the trimer (see "Discussion"). Fig. 6 also shows that the small knobs in the center of the trimer are similar in both types of images and lay just outside the contoured difference.

Analysis of Side View Projections—As side views of trimeric P700·F_A/F_B complexes show an irregular arrangement (due to the asymetric gap between a "sandwich" of two trimers, Fig. 4*A*, *inset*) no image processing of stacked side views can be done. In contrast, in side views of the P700·F_X complex (Fig. 5*A*, *inset*) the (stain filled) gap between two stacked trimers is distinctly smaller and the spacing on both sides of a trimer is about equal. This enables a more precise determination of the height of the P700·F_X complex by image processing. For this purpose 94 projections from PS I complexes in close contact with two neighbors (Fig. 5*A*, marked with *three black arrows*) were repeatedly aligned on

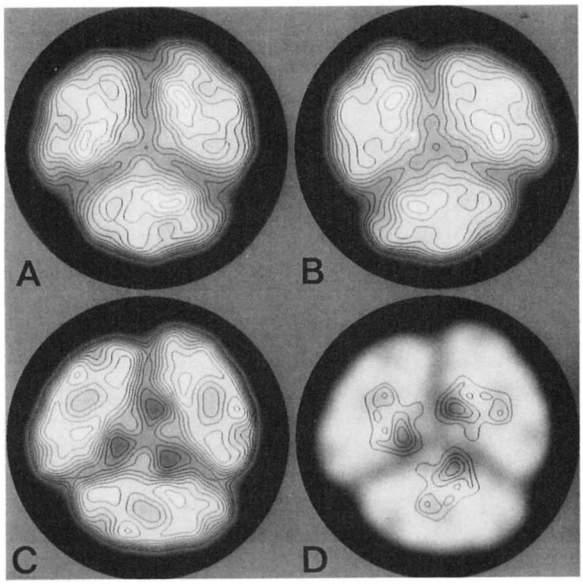

FIG. 6. **Final result of single averaging of *Synechocystis* trimeric PS I projections.** *A*, sum of the best 185 flip projections of the P700·F_A/F_B complex. *B*, sum of the best 65 flop projections of the P700·F_A/F_B complex. *C*, sum of the best 47 flip projections of the P700·F_X complex. *D*, sum of the P700·F_A/F_B complex on which the difference image between *A* and *C* (in the contours only version, with the strongest differences contoured by 4 levels) has been superimposed. All final sums are shown without band-pass filter and on the same scale. The diameter of the circular mask is 20.6 nm.

improved references and, finally, the best 50 aligned images were summed up. The averaged image, Fig. 7, shows only small stain-filled gaps between the complexes. The maximal height of the P700·F_X complex, defined as the center to center distance of the stain maxima on both sides of the projection, was found to be 6.7 nm. For the P700·F_A/F_B complex this distance was found to be 9.2 nm (±0.4 nm, S.D.; n = 40, Fig. 4*A*, *inset*) as determined from printed micrographs. The measurements show that the removal of subunits PsaC, -D, and -E leads to a distinct reduction of the maximal height of PS I by at least 2.5 nm and to the disappearance of the characteristic alternating wide and narrow gaps as seen in rows of aggregated P700·F_A/F_B complexes (Fig. 4*A*, *inset*).

DISCUSSION

Characterization of P700·F_X and P700·F_AF_B Complexes—Since the first report of a cyanobacterial P700·F_X complex preparation (9), more information has been gained concerning the composition of subunits and the function of the redox components of this complex (10–12). Due to the reconstitution capacity of this system the P700·F_X complex became recently a very useful tool for studying the function of stromal proteins with site-directed mutagenesis as has been shown with the mesophilic cyanobacterium *Synechococcus* PCC 6301 (11, 29). In contrast to the function, information about the structure of the P700·F_X complex and especially a detailed comparison with the well characterized structure of the P700·F_A/F_B complex is lacking. The basis for these structural investigations is the development of a new procedure that enables for the first time the isolation of extremely pure and homogeneous monomeric and trimeric P700·F_X complexes from *Synechocystis* PCC 6803. Due to the lack of this structural information, all analytical and functional studies performed up to now with the P700·F_X complex most probably have been done with a mixture of monomeric and trimeric complex (9, 10, 12). The unchanged stability of the trimeric P700·F_X complex purified by us shows that the stromal subunits are not needed for stabilizing the trimer.

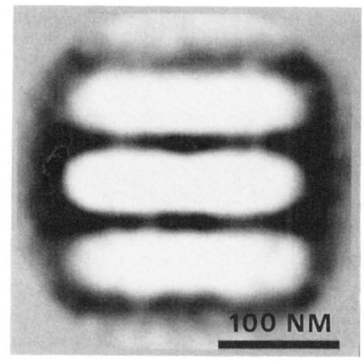

FIG. 7. **Image analysis of side view projections of stacked P700·F_X complexes.** A sum of the best 50 aligned images (out of 94) from P700·F_X complexes in close contact with their neighbors is shown.

The subunit composition of our P700·F_A/F_B complex apparently is similar to the one reported recently by Ikeuchi *et al.* (37) for the same organism. Different is the detection of two forms of PsaF with identical N termini suggesting differences in their C termini. While the existence of two different *PsaF* genes is unlikely (2, 4), it still has to be shown whether these forms of PsaF have a functional role *in vivo* (for instance due to processing) or reflect merely a proteolytical cleavage product. Similar to *Anabaena* (26), PsaF does not cross-react with an antibody against PsaF from higher plants (spinach) suggesting some basic differences between PsaF proteins from cyanobacteria and from higher plants. This is also supported by the observation that plastocyanin from spinach is unable to donate electrons to P700·F_A/F_B complexes from *Synechocystis* (not shown). The observation of a reduced amount of PsaL in the monomers may indicate some role for the structural integrity of the trimer, possibly forming the "connection domain" established by low resolution x-ray crystallography (35).

Our results show that mono- or oligomeric state has neither an influence on recombination half-times nor on antennae size in both PS I complexes. The constant antenna size and the linear dichroism/OD spectra reflect both an unchanged protein environment of the pigments after the urea treatment and the strong binding of chlorophylls by PsaA/B.

Electron Microscopy of Trimeric PS I Complexes—The existence of trimeric P700·F_A/F_B and trimeric P700·F_X complexes is a prerequisite for effective image analysis and enables a direct structural comparison of both complexes with a good signal to noise ratio. The height of the P700·F_A/F_B complex as determined from stacked side view projections is 9.2 nm, which is almost identical with 9.3 ± 0.3 nm (n = 50) as determined for stacks of PS I from *Synechococcus* sp.[3] This value of 9.2–9.3 nm is possibly even slightly higher if the trimers in the double trimer interdigitate to some extent. The height of this complex is in good agreement with 10 nm gained from two-dimensional crystal analysis of the trimeric *Synechococcus* P700·F_A/F_B complex by electron microscopy (18) and with >9 nm derived from analysis of three-dimensional crystals of the same complex by x-ray diffraction (33, 35). The high similarity in these side view dimensions, determined

[3] J. Kruip, E. J. Boekema, D. Bald, A. F. Boonstra, and M. Rögner, unpublished data.

from improved preparations of different cyanobacteria and by different methods, suggests that earlier reports based on analysis by electron microscopy have underestimated the transmembrane dimension of this complex, possibly due to the accidental loss of the three stroma-exposed subunits in the process of sample preparation (15). For spinach preparations (PS I-100, PS I-200) an average height of 6.8 nm was determined from single complexes, due to the lack of stacked side views (31). As the contribution of PsaC, -D, and -E subunit to the side view dimension is hardly to be seen in single complexes and can only be estimated from the distance of stacked side views, the height of these complexes was apparently underestimated.

The difference in height between the P700·F_A/F_B and the P700·F_X complex, 2.5–3.3 nm determined in this report, is in excellent accordance with the 3.5 nm determined for the height of a stroma-exposed protrusion as shown in the 0.6-nm x-ray diffraction model of *Synechococcus elongatus* (33, 35). Concerning the position of PsaC, -D, and -E it should be mentioned, however, that the crystal structure up to now can only indicate the outer shape of the complex; the positioning of these subunits within the complex is not yet possible. By the selective and quantitative removal of the three stroma-exposed subunits (as shown by both analytical and functional studies) and the correlated complete loss of a mass protruding from the membrane surface (as shown by electron microscopy) we can unambiguously and exclusively attribute this mass to these three external subunits and exclude the participation of other subunits to this protrusion.

The flip and flop classes revealed by image analysis of our trimeric P700·F_A/F_B complex have also been found for *S. elongatus* (15), although at a lower resolution. Interestingly, even the features of the monomer, as revealed by analysis of two-dimensional crystals of this organism are very similar (18). However, up to now, it was difficult to speculate which side faces the stroma and which the lumen. As shown in this paper, comparison of top views of trimeric P700·F_A/F_B complexes with analogous structures of trimeric P700·F_X complexes yield further evidence for the orientation of PS I in the membrane. With image analysis of the negatively stained trimeric PS I complexes visualizing details of about 1.5–2 nm, a localization of all PS I subunits with a mass above 10 kDa should be possible (18). The projection of the P700·F_X complex shows a stained oval pit, indicative of an indentation which in analogy to recent three-dimensional models for *S. elongatus* (18, 33, 35) would be located on the lumenal side. Also, the ridge extending in the three-dimensional model from the stromal side corresponds very well with the difference area of Fig. 6*D*. In addition, the similar shape and position of the three small knobs in the center of the trimer in both types of images is consistent with the location of these knobs on the lumenal side of PS I in the three-dimensional model (18). Due to the removal of subunits PsaC/-D/-E the three knobs can clearly be seen in the image of the P700·F_X complex (Fig. 6*C*). Their location suggests a role in the trimer formation.

According to the proposed position of clusters F_A and F_B in the x-ray analysis (33, 35), PsaC should lie in the center of each monomer on a local pseudo 2-fold axis. PsaC in our difference image could therefore be identical with parts of the high density spot in the middle of each PS I monomer. The location of the other two subunits, PsaD and -E, in the difference image is speculation. While it was shown that PsaD can stabilize PsaC (12), the loss of the stroma subunits in the order PsaE > PsaD > PsaC during urea treatment (data not shown) give some evidence that some parts of PsaE could be sitting on top of PsaD. By this arrangement, electron transfer from ferredoxin (bound by PsaD) to the ferredoxin:NADP$^+$ oxidoreductase (possibly bound by PsaE (32)) would be optimized by minimal distances of these components. A location of PsaD underneath of PsaE is also suggested by the strongly reduced accessibility of PsaD by antibodies directed against putative surface-exposed domains in comparison to PsaE (38). Although our results do not rule out a symmetric location of PsaE and PsaD relative to PsaC (2), preliminary results from electron microscopy of a P700·F_AF_B complex lacking PsaE show a rather small contribution of PsaE to the height of the complex.[4] Instead PsaE may cover a large area on top of PS I, thus shielding PsaC and -D.

This report shows that an extremely pure and homogeneous P700·F_X complex preparation enables the localization of the three stroma-exposed subunits PsaC, -D, and -E and thus stimulating the structural analysis of PS I. It is apparent that removal of these subunits does not influence antenna size, the integrity of other subunits or the formation of a stable trimeric complex. The functional integrity of this complex (electron transport from primary donor through to iron-sulfur cluster F_X), and the structural versatility, homogeneous monomeric or trimeric complexes, combined with the ease of scaling up of the developed procedure make these P700·F_X complex preparations potential candidates for PS I crystallization. With respect to the complex structure of the crystallized trimeric PS I complex, highly purified P700·F_X complexes may offer a "minimalized" alternative for structure/function studies with PS I.

Acknowledgments—We thank Prof. Dr. E. Weis and Prof. Dr. E. F. J. van Bruggen for generous support, Dr. J. P. Dekker, J. Van der Lee, and S. Kwa (VU Amsterdam) for help with the spectroscopical characterization of PS I complexes, Dr. E. Schlodder (TU Berlin) for help with the kinetic measurements, Dr. W. Keegstra for his help with computer image analysis, K. Gilissen for photography, and W. Lamkemeyer for excellent technical assistance.

REFERENCES

1. Scheller, H. V., and Moller, B. L. (1990) *Physiol. Plant.* **78,** 484–494
2. Golbeck, J. H., and Bryant, D. A. (1991) *Curr. Top. Bioenerg.* **16,** 83–177
3. Nechushtai, R. (1992) in *Topics in Photosynthesis* (Barber, J., ed) Vol. 11, pp. 443–469, Elsevier, Amsterdam
4. Bryant, D. A. (1992) in *Topics in Photosynthesis* (Barber, J., ed) Vol. 11, pp. 501–549, Elsevier, Amsterdam
5. Zanetti, G., and Merati, G. (1987) *Eur. J. Biochem.* **169,** 143–146
6. Wynn, R. M., Omaha, J., and Malkin, R. (1989) *Biochemistry* **28,** 5554–5560
7. Hippler, M., Ratajczak, R., and Haehnel, W. (1989) *FEBS Lett.* **250,** 280–284
8. Wynn, R. M., and Malkin, R. (1988) *Biochemistry* **27,** 5863–5869
9. Golbeck, J. H., Parrett, K. G., Mehari, T., Jones, K. L., and Brand, J. J. (1988) *FEBS Lett.* **228,** 268–272
10. Li, N., Warren, P. V., Golbeck, J. H., Frank, G., Zuber, H., and Bryant, D. A. (1991) *Biochim. Biophys. Acta* **1059,** 215–225
11. Golbeck, J. H., Mehari, T., Parrett, K., and Ikegami, I. (1988) *FEBS Lett.* **240,** 9–14
12. Li, N., Zhao, J., Warren, P. V., Warden, J. T., Bryant, D. A., and Golbeck, J. H. (1991) *Biochemistry* **30,** 7863–7872
13. Rögner, M., Nixon, P. J., and Diner, B. (1990) *J. Biol. Chem.* **265,** 6189–6196
14. Rögner, M. (1990) *J. Chromat.* **512,** 219–226
15. Boekema, E. J., Dekker, J. P., Rögner, M., Witt, I., Witt, H. T., and van Heel, M. G. (1989) *Biochim. Biophys. Acta* **974,** 81–87
16. Harauz, G., Boekema, E. J., and Van Heel, M. (1988) *Methods Enzymol.* **164,** 35–49
17. Boekema, E. J., Dekker, J. P., van Heel, M. G., Rögner, M., Saenger, W., Witt, I., and Witt, H. T. (1987) *FEBS Lett.* **217,** 283–286
18. Böttcher, B., Gräber, P., and Boekema, E. J. (1992) *Biochim. Biophys. Acta* **1100,** 125–136
19. Ford, R. C., Hefti, A., and Engel, A. (1990) *EMBO J.* **9,** 3067–3075
20. Warren, P. V., Golbeck, J. H., and Warden, J. T. (1993) *Biochemistry* **32,** 849–857
21. Schägger, H., and von Jagow, G. (1987) *Anal. Biochem.* **166,** 368–379
22. Matsudaira, P. (1987) *J. Biol. Chem.* **262,** 10035–10038
23. Rumberg, B., and Witt, H. T. (1964) *Z. Naturforsch.* **19b,** 693–707
24. van der Lee, J., Bald, D., Kwa, S. L. S., van Grondelle, R., Rögner, M., and Dekker, J. P. (1993) *Photosynth. Res.* **35,** 311–321

[4] E. J. Boekema, D. Bald, J. Kruip, B. Lagoutte, and M. Rögner, unpublished data.

25. Okkels, J. S., Scheller, H. V., Svendsen, I., and Moller, B. L. (1991) *J. Biol. Chem.* **266,** 6767–6773
26. Nyhus, K. J., Ikeuchi, M., Inoue, Y., Whitmarsh, J., and Pakrasi, H. B. (1992) *J. Biol. Chem.* **267,** 12489–12495
27. Mühlenhoff, U., Haehnel, W., Witt, H. T., and Hermann R. G. (1993) *Gene* **127,** 71–78
28. Hladik, J., and Sofrova, D. (1991) *Photosynth. Res.* **29,** 171–175
29. Zhao, J., Warren, P. V., Li, N., Bryant, D. A., and Golbeck, J. H. (1990) *FEBS Lett.* **276,** 175–180
30. Rögner, M., Mühlenhoff, U., Boekema, E. J., and Witt, H. T. (1990) *Biochem. Biophys. Acta* **1015,** 415–424
31. Boekema, E. J., Wynn, R. M., and Malkin, R. (1990) *Biochem. Biophys. Acta* **1017,** 49–56
32. Andersen, B., Scheller, H. V., and Moller, B. L. (1992) *FEBS Lett.* **311,** 169–173
33. Witt, H. T., Krauss, N., Hinrichs, W., Witt, I., Fromme, P., and Saenger, W. (1992) in *Research in Photosynthesis, Proceedings of the IX. International Congress on Photosynthesis* (Murata, N., ed) Vol. I, pp. 521–528, Kluwer Academic Publishers, Dordrecht
34. Ikeuchi, M. (1992) *Plant Cell Physiol.* **33,** 669–676
35. Krauss, N., Hinrichs, W., Witt, I., Fromme, P., Pritzkow, W., Dauter, Z., Betzel, C., Wilson, K. S., Witt, H. T., and Saenger, W. (1993) *Nature* **361,** 326–330
36. Bald, D., Kruip, J., Boekema, E. J. and Rögner, M. (1992) in *Research in Photosynthesis, Proceedings of the IX. International Congress on Photosynthesis* (Murata, N., ed) Vol. I, pp. 629–632, Kluwer Academic Publishers, Dordrecht
37. Ikeuchi, M., Sonoike, K., Koike, H., Pakrasi, H. B., and Inoue, Y. (1992) *Plant Cell Physiol.* **33(8),** 1057–1063
38. Lagoutte, B., and Vallon, O. (1992) *Eur. J. Biochem.* **205,** 1175–1185